Author's Accepted Manuscript

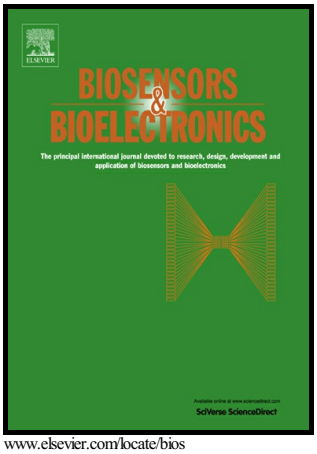

www.elsevier.com/locate/bios

Highly Sensitive Surface-Enhanced Raman Scattering Detection of Hexavalent Chromium based on Hollow Sea Urchin-Like TiO_2@Ag Nanoparticle Substrate

Wen Zhou, Bin-Cheng Yin, Bang-Ce Ye

PII: S0956-5663(16)30796-5
DOI: http://dx.doi.org/10.1016/j.bios.2016.08.036
Reference: BIOS9033

To appear in: *Biosensors and Bioelectronic*

Received date: 15 June 2016
Revised date: 27 July 2016
Accepted date: 13 August 2016

Cite this article as: Wen Zhou, Bin-Cheng Yin and Bang-Ce Ye, Highly Sensitive Surface-Enhanced Raman Scattering Detection of Hexavalent Chromium base on Hollow Sea Urchin-Like TiO_2@Ag Nanoparticle Substrate, *Biosensors an Bioelectronic,* http://dx.doi.org/10.1016/j.bios.2016.08.036

This is a PDF file of an unedited manuscript that has been accepted fo publication. As a service to our customers we are providing this early version o the manuscript. The manuscript will undergo copyediting, typesetting, an review of the resulting galley proof before it is published in its final citable form Please note that during the production process errors may be discovered whic could affect the content, and all legal disclaimers that apply to the journal pertain

ACCEPTED MANUSCRIPT

Highly Sensitive Surface-Enhanced Raman Scattering Detection of Hexavalent Chromium based on Hollow Sea Urchin-Like TiO_2@Ag Nanoparticle Substrate

Wen Zhou[1], Bin-Cheng Yin[1*], and Bang-Ce Ye[1,2*]

[1]Lab of Biosystem and Microanalysis, State Key Laboratory of Bioreactor Engineering, East China University of Science & Technology, Shanghai, 200237, China.

[2]School of Chemistry and Chemical Engineering, Shihezi University, Xinjiang, 832000, China.

binchengyin@ecust.edu.cn

bcye@ecust.edu.cn

[*]Corresponding author.

Abstract

As one of the most toxic heavy metals, hexavalent chromium (Cr(VI)) has long been a concern due to its threats to human health and the environment. In this work, we develop a sensitive surface-enhanced Raman scattering (SERS) sensor for highly specific detection of Cr(VI) using hollow sea urchin-like TiO_2@Ag nanoparticles (NPs). The TiO_2@Ag NPs are functionalized with glutathione (GSH) and used as substrates with 2-mercaptopyridine (2-MPy) as a Raman reporter for a recyclable SERS-active sensor, enabling ultrasensitive detection of Cr(VI). Excellent SERS signals of 2-MPy reporters are detected when GSH complexation with Cr(VI) causes aggregation of the TiO_2@Ag NPs. The developed sensor exhibits good linearity in the range from 10 nM to 2 μM for Cr(VI) with a detection limit of ca. 1.45 nM. It features excellent selectivity to Cr(VI) over other interfering metal ions, and good application for quantitative analysis of Cr(VI) in water samples. Moreover, the proposed SERS sensor can be fully regenerated when exposed to UV light as a result of the self-cleaning ability of the substrates. In contrast to the traditional SERS detection, the present work shed new light on the design and synthesis of hierarchically self-assembled 3D substrate for SERS, catalysis and biosensor development.

Keywords: Hexavalent chromium detection; Surface-enhanced Raman scattering (SERS); Hollow sea urchin-like TiO_2@Ag NPs; Recyclable detection

1. Introduction

Contamination by heavy metals ions has become a serious threat to the environment and living organisms. Among various heavy metals, chromium has been widely used in various industries and has become a major environmental contaminant (Gomez and Callao 2006; Jakubowska 2010; Pellerin and Booker 2000; Sun and Liang 2008). The physicochemical and toxicological properties of chromium depend entirely on its oxidation state (Katz and Salem 1993). Tervalent chromium (Cr(III)) is known as an essential trace element for maintaining normal physiological function, whereas hexavalent chromium (Cr(VI)) is highly carcinogenic and mutagenic, about 100 times more toxic than Cr(III) (Wang et al. 2004), and it universally exists as an oxyanion (CrO_4^{2-}) in aqueous solution (Saha et al. 2011). Therefore, the reduction of Cr(VI), which exist as the chromate anion ($Cr_2O_7^{2-}$) in weakly acidic and basic aqueous solution, to Cr(III) is a crucial process for the detoxification of Cr(VI)-contaminated water and wastewater. According to the United States Environmental Protection Agency (USEPA), the concentration of the total chromium content in drinking water is regulated with a maximum limit of 100 μg/L (Sarkar et al. 2014). Due to the increasing threat of Cr(VI) exposure in the environment, there is a clear unmet need for accurate and reliable method for the determination of Cr(VI). Detection of Cr(VI) has been carried out by a wealth of traditional analytical techniques, including atomic absorption spectrometry (Gardner and Comber 2002; Kiran et al. 2008), spectrofluorometry (Paleologos et al. 2001; Tsuyumoto and Maruyama 2011), spectrophotometry (Themelis et al. 2006; Wu et al. 2013), electrochemistry (Jin et al. 2014; Li et al. 2009), inductively coupled plasma-mass spectrometry (ICP-MS) (Wang et al. 2010). While many of these methods are sensitive and accurate, they are also costly, time-consuming and require tedious sample pretreatments.

As a result of the integration of extraordinary sensitivity, unique spectroscopic fingerprint, and non-destructive data acquisition, surface-enhanced Raman scattering (SERS) has emerged as a promising spectroscopic tool for the identification and detection of the chemical and biological molecules located near/at nanostructured metal surfaces (Dasary et al. 2009; Graham et al. 2008; Lee and Moskovits 2010; Lim et al. 2011; Liu et al. 2012; Shi et al. 2015; Smith 2008; Zheng et al. 2015). SERS has the potential to achieve high sensitivity as well as selectivity toward Cr(VI) (Du and Jing 2011; Ji et al. 2015; Mosier-Boss and Lieberman 2003; Mosier-Boss and Putnam 2013; Xiao et al. 2012). However, because metal ions including Cr(VI) do not exhibit Raman signals, their detection using the SERS technique can only be achieved either via indirect methods that correlate changes in the absolute SERS intensity of a Raman label in the presence of the analyte (Krpetić et al. 2012; Zhang et al. 2013) or by direct detection, in which the nanoatomic ions coordinate an organic chemoreceptor whose SERS spectrum is sensitive to the presence and extent of complexation (Tsoutsi et al. 2013; Tsoutsi et al. 2011).

Most SERS−based Cr(VI) sensing studies use SERS active metallic nanoparticles (Du and Jing 2011; Mosier-Boss and Lieberman 2003; Mosier-Boss and Putnam 2013; Xiao et al. 2012). However, the SERS signal of a single nanomaterial (Au or Ag) is too weak for wide application in ultrasensitive detection. In recent years, researchers have found that a SERS substrate with metallic

Accepted manuscript

ACCEPTED MANUSCRIPT

nanostructure dominate the SERS signal enhancement due to the strong local electromagnetic (EM) field coupling effect of adjacent metal nanostructures (Anker et al. 2008; Genov et al. 2004; Lee et al. 2006; Wang et al. 2005). In addition, it is widely accepted that Raman signals are also closely related to the morphology of SERS substrates. Therefore, metals with different architectures have been widely constructed to obtain effective SERS active-substrate (Shen et al. 2008; Yoon et al. 2008). Among various architectures, 3D nanostructures (such as flower-like (Wang et al. 2011), star-like (Kumar et al. 2007), sea urchin-like (Bakr et al. 2006; Lu et al. 2008) and dendritic morphologies (Ren et al. 2012)) are far superior because their 3D spatial structures can generate more active "hot spots" (Ko and Tsukruk 2008; Zhang et al. 2008), and several novel properties. In particular, a new family of 3D substrates, sea urchin-like hollow nanostructure decorated with metal NPs, possess a high surface-to-volume ratio, and rich surface tips. Their open morphology preserves the large active surface area and the interstitial channels for diffusion of probe molecules into the structure, thereby improving the efficiency of surface reactions (Zhu et al. 2008). Therefore, they are very appropriate for assembling as a SERS sensor. Despite these amazing advances, it should be emphasized that most of these SERS substrates are discarded after one detection because they cannot be recycled. The combination of noble metals and semiconductor materials as recyclable SERS substrates has been proved to be an effective way of solving the problem described above (Esmaielzadeh Kandjani et al. 2014; Shan et al. 2015; Zhang et al. 2015).

Recently, due to its remarkable physical and chemical properties, TiO_2 has been applied in photocatalysis, pollutant degradation and even analytic detection (Es-Souni et al. 2010). It has been reported that TiO_2 can be exploited as a potential candidate for the fabrication of SERS substrates (Ji et al. 2011; Musumeci et al. 2009). Furthermore, efforts have also been dedicated to fabricate hybrids consisting of TiO_2 and Ag/Au NPs to obtain a synergic effect of electromagnetic (EM) and charge transfer (CT) enhancements, also to exploit high surface area with increasing amount of adsorbed molecules (Lamberti et al. 2015; Tan et al. 2012), and these hybrids can serve as recyclable SERS-active substrates for photocatalysis under UV light irradiation (Li et al. 2010; Zou et al. 2013).

In the present work, we use the characteristics of sea urchin-like TiO_2@Ag nanostructures to prepare a multifunctional SERS-active substrates (Li et al. 2015; Su et al. 2014), which can be applied to the recyclable SERS detection. We propose a simple and efficient protocol for the synthesis of sea urchin-like TiO_2@Ag nanostructures, and demonstrate their application as novel SERS-active substrates for Cr(VI) detection based on a "signal-amplification" strategy capable of generation for multiple sensing events. The design and fabrication of stable, homogeneous, reproducible and recyclable TiO_2@Ag hybrids is achieved via a hydrothermal reaction of SiO_2@TiO_2 core-shell microspheres in the presence of NaOH to form hollow sea urchin-like TiO_2 NPs. Then, Ag NPs are deposited on the TiO_2 surface, resulting in a strong local surface plasmon resonance (LSPR) absorption strength and highly sensitive SERS enhancement. The sensitivity and reproducibility of the substrate were investigated by applying Rhodamine 6G (R6G) as a Raman reporter molecule. Quantitative determination of Cr(VI) was achieved using a portable Raman spectrometer, based on the functionalization of the hollow TiO_2@Ag NPs with glutathione (GSH) and 2-mercaptopyridine (2-MPy). When moderate amount of GSH and 2-MPy are present, the TiO_2@Ag NPs keep in a state of suspension. However, the presence of Cr(VI) would lead to the aggregation of TiO_2@Ag NPs to form many SERS "hot spots", and significant SERS enhancement signals of the Raman reporter molecule, 2-MPy. Our proposed SERS sensor features high sensitivity, reproducibility and selectivity, and exhibits a limit of detection (LOD) for Cr(VI) of ca. 1.45 nM. The practicality of this proposed method was further validated through the detection of Cr(VI) in water samples.

2. Materials and methods

2.1. Chemicals and reagents

Tetraethyl orthosilicate (TEOS, 99%), tetrabutyl titanate (TBOT, 99%), Glutathione (GSH, 98.0%) and silver nitrate ($AgNO_3$, 99.8%) were purchased from Sigma-Aldrich; Anhydrous ethanol, polyethylene glycol (PEG, MW 6 000), ammonium hydroxide ($NH_3 \cdot H_2O$, 28%), hydrochloric acid (HCl, 36.5%), sodium hydroxide, trisodium citrate, potassium dichromate ($K_2Cr_2O_7$) were of analytical grade and obtained from Sinopharm Chemical Reagent Co., Ltd. (Shanghai, China). Rhodamine 6G (R6G) and 2-mercaptopyridine (2-MPy) were purchased from Solarbio and were used without further purification. Milli-Q water produced by a Milli-Q system (Millipore, Bedford, MA) was used in all experiments. The real samples of river water were collected from East China University of Science and Technology, Shanghai, China.

2.2. Instrumentation

To demonstrate the overall uniformity and morphology of the particles, the samples were examined by transmission electron microscopy (TEM, JEM-1400) and high-resolution transmission electron microscopy (HRTEM, JEM-2100). The samples for the TEM measurements were suspended in ethanol and supported onto a Cu grid. The crystalline structure was investigated by X-ray powder diffraction (XRD; Rigaku D/max 2550 VB/PC, Japan), in a 2θ range from 10° to 80°, using Cu Kα radiation. The optical absorption spectra were acquired on a UV−vis spectrometer (Shimadzu UV-1800, Japan). During the photocatalytic processes, a 15 W mercury lamp with maximum emission of 365 nm was used as the UV light source. Raman spectra were collected on a portable Raman spectrometer (B&W Tek Instruments, USA) equipped with a 785 nm laser, a charge-coupled device (CCD) detector and a 40 × objective lens with numerical aperture (NA) 0.65. The acquisition and analysis of Raman data were performed by using the BWSpec4 software.

2.3. Preparation of sea urchin-like TiO_2 nanoparticles

The monodisperse SiO_2@TiO_2 core-shell nanospheres were obtained through a templating approach. First, colloidal SiO_2 particles were prepared based on a typical ammonia-catalyzed Stöber method. A mixture of 3 mL of $NH_3 \cdot H_2O$ solution (28%), 3 mL of deionized water and 19 mL of absolute ethanol was stirred vigorously for 20 min. Then, a TEOS solution prepared by dispersing 1.3 mL of TEOS into 3.7 mL of absolute ethanol was quickly introduced into the above system, and the sol-gel process was allowed to proceed under agitation for 2 h at

Accepted manuscript

ACCEPTED MANUSCRIPT

room temperature. The precipitated SiO_2 was then separated by centrifugation and washed with deionized water and ethanol, followed by drying at 60 °C for 6 h under vacuum. For the TiO_2 coating, 0.06 g of the obtained SiO_2 nanospheres was redispersed in 40 mL of absolute ethanol by ultrasound, followed by the addition of 0.3 mL of $NH_3 \cdot H_2O$ solution (28%). The mixture was transferred to a flask and stirred mechanically for 15 min at 45 °C. A mixture of 0.8 mL of TBOT with 20 mL of absolute ethanol was added dropwise to the suspension with continuous stirring to form an emulsion, and the final mixture was aged at 45 °C for 24 h under continuous mechanical stirring. The resultant products were then separated and collected by centrifugation, and washed 3 times with deionized water and ethanol, respectively. The obtained powders were dried at 60 °C for 6 h under vacuum. Subsequently, 0.06 g of the resulting nanospheres was mixed with 40 mL of NaOH solution (2.0 M) using magnetic stirring for 4 h to remove SiO_2 cores. The mixture was then transferred to a Teflon-lined stainless steel autoclave (50 mL capacity), and was hydrothermally treated at 120 °C for 2 h, followed by cooling to room temperature. The as-prepared products were thoroughly washed with water 3 times to remove any ionic impurities, and dried at 60 °C for 6 h under vacuum. Finally, to obtain a highly crystalline anatase phase, 0.04 g of titanate hollow nanoparticles was immersed in 10 mL HCl (0.1 M) for 20 min, and then washed with deionized water until neutral, followed by a calcination process in air at 450 °C for 4 h to remove all organic compounds and crystallize the anatase TiO_2.

2.4. Synthesis of Ag nanoparticle-decorated TiO_2 nanoparticles

For the preparation of TiO_2@Ag NPs, in a typical synthesis, 40 mg of the previously prepared hollow TiO_2 spheres were soaked in 50 mL deionized water, followed by adding 9 mg of $AgNO_3$, and the solution was stirred by a magnetic stirrer at 60 °C for 30 min. Subsequently, 0.8 mL of sodium citrate (1 wt%) aqueous solution was added slowly into the system, and the reaction proceeded for 1 h in a water bath at 90 °C under magnetic stirring. The final black products were collected by centrifugation and washed 3 times with deionized water and ethanol, then dried at 45 °C for 8 h under vacuum.

2.5. Functionalization of TiO_2@Ag NPs

The GSH and 2-MPy functionalization of TiO_2@Ag NPs was accomplished following a simple procedure. In brief, an aliquot of TiO_2@Ag NPs was dispersed in 1 mL of PEG (8%, MW 6 000) to keep the nanoparticles suspended. Then, the TiO_2@Ag NPs surfaces were modified by the addition of 100 µL GSH (100 µM), 400 µL 2-Mpy (500 µM), to the above TiO_2@Ag NPs colloid in phosphate buffer (pH 6.5) with shaking for 2 h at 4 °C.

2.6. SERS detection of Cr(VI)

For detection of Cr(VI), various concentrations of Cr(VI) (2 nM~12 µM) were prepared using serial dilution of a $K_2Cr_2O_7$ stock solution. Briefly, 200 µL of Cr(VI) at a series of different concentrations was mixed with 1.0 mL of the as-prepared GSH/2-Mpy-modified TiO_2@Ag NPs colloid. After incubating in 0.1 M phosphate buffered saline (PBS, pH 7.4) solution at 4 °C for 20 min, the TiO_2@Ag NPs were centrifugated at 10 000 rpm for 3 min and the supernatant was removed to give a residual volume of 20 µL. Afterwards, 10 µL of the residual TiO_2@AgNPs solution was deposited on a cleaned silica slide and air-dried as SERS substrates for further SERS measurement.

3. Results and discussion

3.1. Synthesis of sea urchin-like TiO_2@Ag nanospheres

As illustrated in Scheme 1, the hollow sea urchin-like TiO_2@Ag nanospheres were designed strategically and fabricated by a multistep protocol. Schematically, the SiO_2 nanoparticles were first synthesized via a modified Stöber method (Rao et al. 2005). The TiO_2 shell layer was then grown on the surface of SiO_2 nanospheres through a controlled sol-gel process, in which tetrabutyl titanate (TBOT) was hydrolyzed and condensed in ethanol/ammonia alkaline solution (Joo et al. 2012; Li et al. 2012). After a hydrothermal treatment of SiO_2@TiO_2 core-shell nanospheres in NaOH aqueous solution at 120 °C for 2 h, a novel sea urchin-like yolk-shell structure with radially extending nanofibers was obtained. Afterwards, a highly crystalline TiO_2 with sea urchin-like morphology was obtained through acid-treatment of the titanate followed by calcination. Finally, Ag NPs were loaded on the nanofibers of the nanoparticles via in situ reduction of $AgNO_3$ with trisodium citrate.

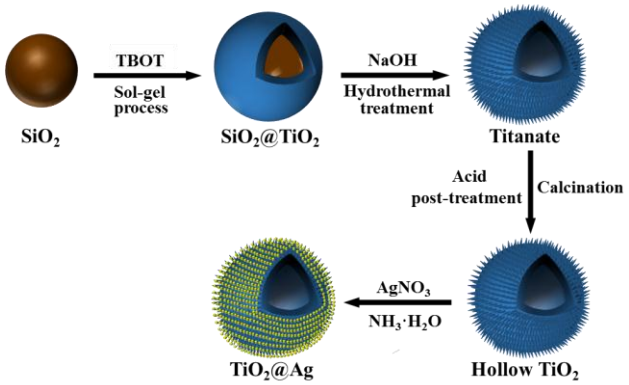

Scheme 1. Schematic illustration of the Fabrication of Hollow Sea Urchin-Like TiO_2@Ag NPs.

Accepted manuscript

ACCEPTED MANUSCRIPT

3.2. Characterization of nanoparticle substrate

The morphologies and structure of the as-prepared nanospheres at various stages in the synthesis process were first examined by TEM. As shown in Fig. 1A, the SiO_2 nanoparticles with an average diameter of 200 nm display a well-defined spherical or sphere-like structure. A uniform shell of TiO_2 with a thickness of about 85 nm was coated onto SiO_2 cores, which ensures the degradation of analyte so that the SERS substrates can be re-used. After treatment in a solution of NaOH, the SiO_2 cores were largely dissolved through etching, generating a sea urchin-like hollow structure about 600 nm in diameter. The nanofibers of the outer shell possess an average length of 95 nm. Additionally, HRTEM images revealed that the overall morphology of as-prepared TiO_2@Ag NPs was almost maintained and that Ag nanoparticles with an average size of 40 ± 8 nm were finely dispersed on the surface of the TiO_2 hollow spheres.

The crystal structure and phase purity of the as-synthesized products were identified by X-ray diffraction (XRD). As shown in Fig. 1B, the as-prepared SiO_2@TiO_2 sample exhibits a broad peak between 20° and 30°, which is the background peak attributed to the glass slide. No other diffraction peaks are observed in the pattern, indicating that the SiO_2@TiO_2 sample is amorphous. After calcination at 450 °C for 4 h, the XRD pattern shows new characteristic diffraction peaks that can be accurately assigned to the anatase phase of TiO_2 (JCPDS card No. 21-1272), indicating that the nanostructures are highly pure. Although Ag peaks are located at most the same 2θ angles as anatase phase, four characteristic peaks of Ag displayed in the pattern of TiO_2@Ag NPs can be distinguished and indexed as the (111), (200), (220), and (311) planes. Fig. 1C shows the corresponding diffuse-reflectance absorption spectra of the as-obtained SiO_2@TiO_2, hollow sea urchin-like TiO_2, Ag NPs and TiO_2@Ag NPs hybrids. SiO_2@TiO_2 yields an absorption peak in the UV region around 296 nm, which is assigned to the characteristic absorption peak of TiO_2. The sea urchin-like hollow TiO_2 exhibits broad absorption in the visible light region, which can be ascribed to the characteristic of anatase phase and hollow structure (Syoufian et al. 2007; Yu et al. 2007). The Ag NPs exhibit a strong and sharp LSPR at wavelengths around 414 nm. However, it is a remarkable fact that after Ag NPs were loaded on the hollow TiO_2, the LSPR wavelength is significantly red-shifted about 78 nm and prominent absorption in 400~800 nm wavelength range is observed, indicating effective surface plasmonic couplings produced between the metallic Ag nanocrystals and anatase-TiO_2 (Tsoutsi et al. 2013). As a result, the developed SERS substrates feature much stronger Raman signals than the pure Ag NPs (Fig. S1). The deposition density of Ag NPs was optimized by changing the concentrations of $AgNO_3$, and the SERS properties are displayed in Fig. S2. The significant SERS enhancement of the sea urchin-like hollow TiO_2@Ag NPs substrates is primarily ascribed to the local electromagnetic effect. The charge transfer from Ag to TiO_2 results in the formation of an internal electric field, and causes the formation of local electric fields around the Ag NPs. The surface plasmon resonance (SPR) can enhance the localized electromagnetic field and improve the Raman scattering of the analytes. Moverover, the abundant needle-shaped nanofiber structures on the surface of sea urchin-like hollow TiO_2@Ag NPs can uninterruptedly amplify the surface plasmon excitation; resulting in the further increase of SERS signals. Besides, the high aspect ratio of the sea urchin-like TiO_2@Ag NPs hybrids is obviously larger than that of a flat surface of the same area, which may lead to contacting with more probe molecules, thus lead to the enhancement of SERS. Typically, as shown in Fig. 1D, the prominent SERS intensity of R6G with different concentrations (from 10^{-12} M to 10^{-6} M) adsorbed on the optimal TiO_2@Ag NPs was measured. The characteristic peaks of R6G can be identified clearly even at a concentration as low as 10^{-12} M, and the enhancement factor (EF) of the sea urchin-like TiO_2@Ag NPs was calculated to be 7.6×10^6 (see the Supporting Information for a detailed calculation of EF). Furthermore, the prepared SERS-active substrates can be recycled and still show significant photocatalytic activity. As shown in Fig. S3, the remarkable photocatalytic capability of TiO_2@Ag NPs could be employed to degrade the R6G molecules after performing SERS analysis once, and then the TiO_2@Ag NPs substrates could be used for the further detection.

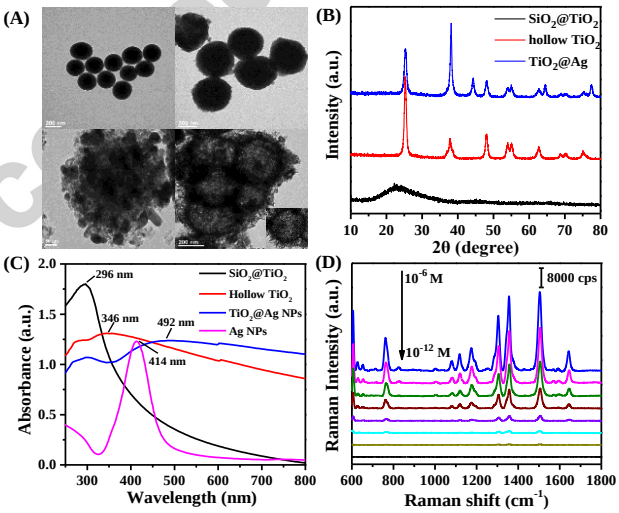

Fig. 1. (A) Characterizations of the nanoparticles at various stages of the synthesis process, including (A) TEM images of SiO_2, SiO_2@TiO_2, hollow TiO_2, and TiO_2@Ag NPs (clockwise from top left). (B) XRD patterns of SiO_2@TiO_2, hollow TiO_2, and TiO_2@Ag NPs. (C) UV−visible spectra of the as-prepared SiO_2@TiO_2, hollow TiO_2, TiO_2@Ag NPs and Ag NPs. (D) Raman spectra of R6G molecules (from 10^{-12} M to 10^{-6} M) from the surface of TiO_2@Ag NPs substrate. SERS detection parameters: $\lambda_{excitation}$ = 785 nm, accumulation time = 10 s, laser power = 100 mW.

3.3. Working principle of Cr(VI) detection

Accepted manuscript

ACCEPTED MANUSCRIPT

Scheme 2 schematically illustrates the mechanism for Cr(VI) detection using sea urchin-like TiO_2@Ag NPs together with GSH and 2-MPy. A certain concentration of buffer salt solution can destroy the stability of the TiO_2@Ag NPs, and consequently lead to aggregation of the nanoparticles. It has been reported that glutathione (GSH), a thiol−containing oligopeptide (γ-Glu-Cys-Gly) can bind to TiO_2@Ag NPs through Ag−S bonds (Chen et al. 2010). Polypeptide have a good protective effect on Ag NPs, therefore GSH can effectively prevent the nanoparticles from salt-induced aggregation. Moreover, it can act as a ligand and bind to Cr(VI) through the formation of Cr(VI)-GSH complexes (Gaggelli et al. 2002; Grill et al. 1985; Zhang et al. 2009), which would destroy the stability of the GSH-functionalized TiO_2@Ag NPs and lead to aggregation. The Raman reporters of 2-MPy are labeled on the Ag NP surfaces through two possible binding sites, the mercapto group and the amino group (Baldwin et al. 1997; Nalbant Esenturk and Hight Walker 2009). Before the experiment, the unmodified TiO_2@Ag NPs colloid is first stabilized by a stabilizer PEG 6000 (8%) coating on the NPs surfaces (Fig. S4) (Zhang et al. 2012). In the absence of Cr(VI), the GSH-modified TiO_2@Ag NPs colloid remain in a well-dispersed state. On the contrary, in the presence of Cr(VI), the formation of metal sulfide-phytochelatin lead to dramatic aggregation of nanoparticles which is visible to the naked eye. The aggregated TiO_2@Ag NPs SERS-active substrates can produce a number of "hot spots", and thus strong SERS enhancement signal of 2-MPy is obtained.

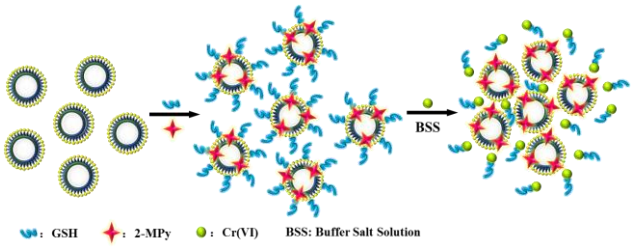

Scheme 2. Schematic Representation of SERS Sensing Strategy for Cr(VI) Detection.

3.4. Investigation of the feasibility

As shown in Fig. 2, control experiments were performed to verify the feasibility of the SERS sensing for Cr(VI) detection. In the absence of 2-MPy, no SERS signal was observed (curve a−c). In the presence of 2-MPy and GSH, there was no apparent SERS signal (curve d, e). However, several intense peaks were obtained in the simultaneous presence of Cr(VI), 2-MPy and GSH-modified TiO_2@AgNPs (curve f), demonstrating that the indirect SERS sensing method using 2-MPy as a Raman reporter is feasible for Cr(VI) analysis.

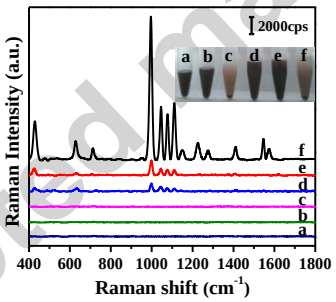

Fig. 2. SERS spectra corresponding to (a) nonaggregated unmodified TiO_2@Ag NPs in the absence of Cr(VI), (b) nonaggregated GSH-modified TiO_2@Ag NPs in the absence of Cr(VI), (c) aggregated GSH-modified TiO_2@Ag NPs in the presence of 1.0 μM Cr(VI), (d) nonaggregated 2-MPy-modified TiO_2@Ag NPs in the absence of Cr(VI), (e) nonaggregated GSH/2-MPy-modified TiO_2@Ag NPs in the absence of Cr(VI) and (f) aggregated GSH/2-MPy-modified TiO_2@Ag NPs in the presence of 1.0 μM Cr(VI). The inset shows the corresponding sample photographs.

3.5. Optimization of experimental conditions

In order to acquire satisfactory SERS intensities and useful analytical results, several parameters were optimized. First, the effect of the concentration of 2-MPy on SERS signal intensity was investigated. Six different concentrations of 2-MPy ranging from 10^{-9} M to 8×10^{-7} M were tested, and the corresponding Raman spectra and a blank control spectrum were recorded in Fig. S5. The SERS signal intensity increased as the concentration of 2-MPy increased with largest signal produced at 2×10^{-7} M (Fig. S6A). Further increase in the concentration of 2-MPy resulted in a decline in signal enhancement. Moreover, a higher concentration of 2-MPy also induced some nanoparticles aggregation. Thus, 2×10^{-7} M of 2-MPy was applied throughout the remaining work. The influence of GSH concentration on the SERS signal intensity was also investigated. As shown in Fig. S6B, the SERS signal became more intense with increasing GSH concentration up to 6×10^{-7} M. A higher concentration of GSH led to aggregation of TiO_2@Ag NPs. Thus, 6×10^{-7} M of GSH was used throughout the rest of the work.

3.6. Sensitivity investigation

Accepted manuscript

ACCEPTED MANUSCRIPT

Under the above optimized conditions, the SERS spectra of 2-MPy produced from GSH-modified TiO_2@AgNPs with different concentrations of Cr(VI) were recorded to determine the sensitivity. As shown in Fig. 3A and B, pronounced SERS bands of 2-MPy at 433, 634, 1002, 1050, 1083, 1114, 1413 and 1551 cm^{-1} were unambiguously observed in the presence of Cr(VI). In addition, the SERS intensity increased as a function of Cr(VI) concentration, indicating that more 2-MPy-labeled GSH-TiO_2@Ag NPs were aggregated with increasing concentration of Cr(VI). Fig. 3C shows that the intensity of the 1002 cm^{-1} peak increased as the concentration of Cr(VI) increased, and a satisfactory linear relationship was obtained for Cr(VI) concentrations up to 2 μM (R^2 = 0.996) as shown in the inset of Fig. 4C. The limit of detection based on a signal-to-noise ratio of 3 was estimated to be 1.45 nM (about 75.4 ng/L, see the Supporting Information for a detailed calculation of LOD), which is much lower than the maximum contaminant level for Cr(VI) in drinking water 100 μg/L defined by USEPA. In addition, compared to the reported nanomaterial-based methods, our proposed SERS sensor also offers a high sensitivity for Cr(VI) determination (Table S1). In order to verify that the SERS sensor is suitable for sensitive and specific detection of Cr(VI) in practical applications, the detection of Cr(VI) in real samples (tap water and lake water) was investigated (Fig. S7). The data listed in Table S2 indicates that, when the known amount of Cr(VI) was added to these samples, the recovery of Cr(VI) ranged from 94.8% to 109.8%. These results confirm that the proposed SERS sensor has high accuracy, reliability, and sensitivity to meet the requirements of the application.

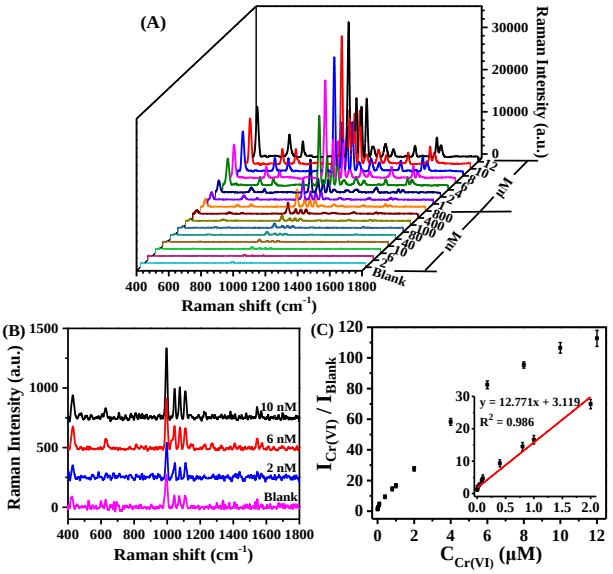

Fig. 3. (A) SERS spectra of 2-MPy for quantitative evaluation of Cr(VI) with different concentrations. Blank stands for the absence of Cr(VI). (B) SERS spectra of 2-MPy for quantitative evaluation of Cr(VI) at low concentrations (2 nM, 6 nM, and 10 nM). (C) The curves of Raman intensity at 1002 cm^{-1} changes upon the addition of different concentrations of Cr(VI). Inset shows a linear relationship in the lower concentration range from 10 nM to 2 μM (R^2 = 0.986). The error bar represents standard deviation based on three independent measurements. SERS detection parameters: $\lambda_{excitation}$ = 785 nm, accumulation time = 10 s, laser power = 50 mW.

3.7. Selectivity and regeneration test

To investigate the specificity of the SERS sensor for Cr(VI) detection, several typical metal ions were further examined by parallel assays, including Al^{3+}, Ca^{2+}, Co^{2+}, Cr^{3+}, Cu^{2+}, Fe^{3+}, K^{+}, Mg^{2+}, Mn^{2+}, Ni^{2+}, Pb^{2+}, and Zn^{2+} at a concentration of 10 μM. As shown in Fig. 4A, only feeble SERS intensities were observed for metal ions other than Cr(VI) due to their low binding affinity to GSH. Among these metal ions except Cr(VI), a higher response was observed in Cu^{2+} and Pb^{2+}. It is because the formation of coordination complexes between Cu^{2+} and GSH through -NH_2 group, and Pb^{2+} and GSH through -COOH group, would lead to a slight aggregation of nanoparticles (Beqa et al. 2011; Fang and Zhou 2003), resulting in weak SERS signals. While distinct SERS enhancement was observed with the addition of 2 μM Cr(VI), indicating excellent selectivity of the developed SERS sensors for Cr(VI) detection. For direct quantitative comparison, corresponding Raman intensities of the 1002 cm^{-1} peak of 2-MPy in the presence of the above substances are presented as histograms in Fig. 4B.

Because most of the current SERS sensors for the determination of Cr(VI) usually cannot be used more than once, it is highly desirable to fabricate a recyclable Cr(VI) SERS sensor. As shown in Fig. S8, the photocatalytic activity of the fabricated SERS substrate for the degradation of Cr(VI) under UV light irradiation was verified. By a simple photodegradation and rinsing process, all the analytes can be completely removed from the surface of SERS substrates (see the Supporting Information for the experimental details). As shown in Fig. 4C, over 5 cycles of surface regeneration experiment, the SERS intensity of the 1002 cm^{-1} peak for 2-MPy varied by less than 8%, indicating that the developed surfaces can be fully regenerated repeatedly following Cr(VI) sensing/degradation events.

Accepted manuscript

ACCEPTED MANUSCRIPT

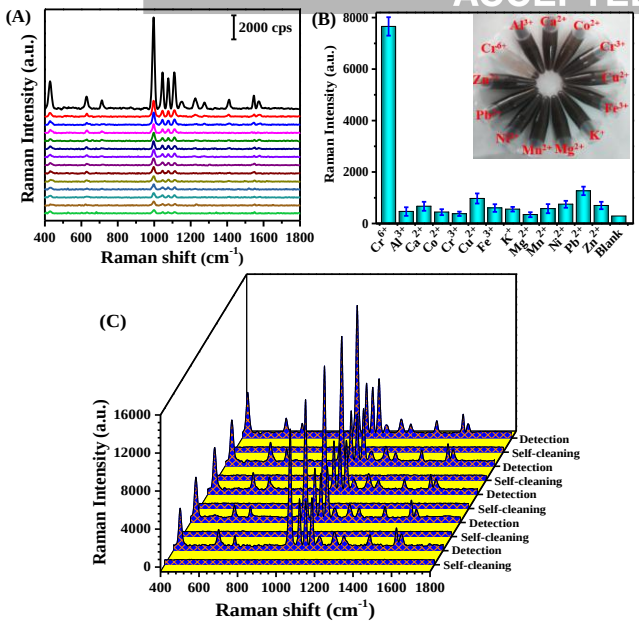

Fig. 4. (A) Selectivity of the present sea urchin-like TiO_2@Ag NPs SERS-active substrate detection on Cr(VI) (2 μM) and other kinds of metal ions (Al^{3+}, Ca^{2+}, Co^{2+}, Cr^{3+}, Cu^{2+}, Fe^{3+}, K^+, Mg^{2+}, Mn^{2+}, Ni^{2+}, Pb^{2+}, and Zn^{2+}, 10 μM for each ions). (B) The corresponding SERS intensity of the 1002 cm^{-1} peak was utilized for comparison. The error bar represents standard deviation based on three independent measurements. (C) Raman spectra of five detection/UV light cleaning cycles of 3 μM Cr(VI). Each cycle consists of adsorption of the target solution followed by UV light irradiation. The graph shows the Raman spectra before and after cleaning.

4. Conclusion

In summary, we have presented a new SERS sensing strategy for highly sensitive, specific, and reproducible detection of Cr(VI), based on the use of a novel sea urchin-like TiO_2@Ag NPs nanostructure. The presence of Cr(VI) induces TiO_2@Ag NPs aggregation through the coordination of GSH to Cr(VI). The high-quality sensor allows high sensitivity and selectivity for Cr(VI) over other interfering metal ions. Moreover, the SERS sensor features good recyclability due to the excellent self-cleaning ability of the TiO_2@Ag NPs. We further demonstrated that the SERS sensor is capable of analyzing Cr(VI) in lake and tap water samples with good accuracy. We envisage that the present strategy can be modified for analysis of some other toxic metal ions in environmental and biological samples.

Acknowledgments

This work was jointly supported by the National Natural Science Foundation of China (Grants 21335003, 21575089) and the Fundamental Research Funds for the Central Universities.

References

Anker, J.N., Hall, W.P., Lyandres, O., Shah, N.C., Zhao, J., Van Duyne, R.P., 2008. Nat. Mater. 7(6), 442-453.

Bakr, O.M., Wunsch, B.H., Stellacci, F., 2006. Chem. Mater. 18(14), 3297-3301.

Baldwin, J.A., Vlčková, B., Andrews, M.P., Butler, I.S., 1997. Langmuir 13(14), 3744-3751.

Beqa, L., Singh, A.K., Khan, S.A., Senapati, D., Arumugam, S.R., Ray, P.C., 2011. ACS Appl. Mater. Interfaces 3(3), 668-673.

Chen, Z., He, Y., Luo, S., Lin, H., Chen, Y., Sheng, P., Li, J., Chen, B., Liu, C., Cai, Q., 2010. Analyst 135(5), 1066-1069.

Dasary, S.S., Singh, A.K., Senapati, D., Yu, H., Ray, P.C., 2009. J. Am. Chem. Soc. 131(38), 13806-13812.

Du, J., Jing, C., 2011. J. Colloid Interface Sci. 358(1), 54-61.

Es-Souni, M., Es-Souni, M., Habouti, S., Pfeiffer, N., Lahmar, A., Dietze, M., Solterbeck, C.H., 2010. Adv. Funct. Mater. 20(3), 377-385.

Esmaielzadeh Kandjani, A., Sabri, Y.M., Mohammad-Taheri, M., Bansal, V., Bhargava, S.K., 2014. Environ. Sci. Technol. 49(3), 1578-1584.

Fang, C., Zhou, X., 2003. Electroanalysis 15(20), 1632-1638.

Gaggelli, E., Berti, F., D'Amelio, N., Gaggelli, N., Valensin, G., Bovalini, L., Paffetti, A., Trabalzini, L., 2002. Environ. Sci. Technol. 110(5), 733.

Gardner, M., Comber, S., 2002. Analyst 127(1), 153-156.

Genov, D.A., Sarychev, A.K., Shalaev, V.M., Wei, A., 2004. Nano Lett. 4(1), 153-158.

Gomez, V., Callao, M., 2006. TrAC, Trends Anal. Chem. 25(10), 1006-1015.

Accepted manuscript

ACCEPTED MANUSCRIPT

Graham, D., Thompson, D.G., Smith, W.E., Faulds, K., 2008. Nat. Nanotechnol. 3(9), 548-551.

Grill, E., Winnacker, E.-L., Zenk, M.H., 1985. Science 230(4726), 674-676.

Jakubowska, M., 2010. J. Hazard. Mater. 176(1), 540-548.

Ji, W., Wang, Y., Tanabe, I., Han, X., Zhao, B., Ozaki, Y., 2015. Chem. Sci. 6(1), 342-348.

Ji, W., Xue, X., Ruan, W., Wang, C., Ji, N., Chen, L., Li, Z., Song, W., Zhao, B., Lombardi, J.R., 2011. Chem. Commun. 47(8), 2426-2428.

Jin, W., Wu, G., Chen, A., 2014. Analyst 139(1), 235-241.

Joo, J.B., Zhang, Q., Lee, I., Dahl, M., Zaera, F., Yin, Y., 2012. Adv. Funct. Mater. 22(1), 166-174.

Katz, S.A., Salem, H., 1993. J. Appl. Toxicol. 13(3), 217-224.

Kiran, K., Kumar, K.S., Prasad, B., Suvardhan, K., Lekkala, R.B., Janardhanam, K., 2008. J. Hazard. Mater 150(3), 582-586.

Ko, H., Tsukruk, V.V., 2008. Small 4(11), 1980-1984.

Krpetić, Ž., Guerrini, L., Larmour, I.A., Reglinski, J., Faulds, K., Graham, D., 2012. Small 8(5), 707-714.

Kumar, P.S., Pastoriza-Santos, I., Rodríguez-González, B., de Abajo, F.J.G., Liz-Marzan, L.M., 2007. Nanotechnology 19(1), 015606.

Lamberti, A., Virga, A., Chiadò, A., Chiodoni, A., Bejtka, K., Rivolo, P., Giorgis, F., 2015. J. Mater. Chem. C 3(26), 6868-6875.

Lee, S.J., Morrill, A.R., Moskovits, M., 2006. J. Am. Chem. Soc. 128(7), 2200-2201.

Lee, S.J., Moskovits, M., 2010. Nano Lett. 11(1), 145-150.

Li, J., Tan, L., Wang, G., Yang, M., 2015. Nanotechnology 26(9), 095601.

Li, J., Zhang, J., Wei, H., Wang, E., 2009. Analyst 134(2), 273-277.

Li, W., Yang, J., Wu, Z., Wang, J., Li, B., Feng, S., Deng, Y., Zhang, F., Zhao, D., 2012. J. Am. Chem. Soc. 134(29), 11864-11867.

Li, X., Chen, G., Yang, L., Jin, Z., Liu, J., 2010. Adv. Funct. Mater. 20(17), 2815-2824.

Lim, D.-K., Jeon, K.-S., Hwang, J.-H., Kim, H., Kwon, S., Suh, Y.D., Nam, J.-M., 2011. Nat. Nanotechnol. 6(7), 452-460.

Liu, R., Liu, B., Guan, G., Jiang, C., Zhang, Z., 2012. Chem. Commun. 48(75), 9421-9423.

Lu, L., Ai, K., Ozaki, Y., 2008. Langmuir 24(3), 1058-1063.

Mosier-Boss, P., Lieberman, S., 2003. Langmuir 19(17), 6826-6836.

Mosier-Boss, P., Putnam, M., 2013. Anal. Chim. Acta 801, 70-77.

Musumeci, A., Gosztola, D., Schiller, T., Dimitrijevic, N.M., Mujica, V., Martin, D., Rajh, T., 2009. J. Am. Chem. Soc. 131(17), 6040-6041.

Nalbant Esenturk, E., Hight Walker, A., 2009. J. Raman Spectrosc. 40(1), 86-91.

Paleologos, E., Stalikas, C., Tzouwara-Karayanni, S., Karayannis, M., 2001. Anal. Chim. Acta 436(1), 49-57.

Pellerin, C., Booker, S.M., 2000. Environ. Health Perspect. 108(9), 402-407.

Rao, K.S., El-Hami, K., Kodaki, T., Matsushige, K., Makino, K., 2005. J. Colloid Interface Sci. 289(1), 125-131.

Ren, W., Zhu, C., Wang, E., 2012. Nanoscale 4(19), 5902-5909.

Saha, R., Nandi, R., Saha, B., 2011. J. Coord. Chem. 64(10), 1782-1806.

Sarkar, S., Dutta, S., Bairi, P., Pal, T., 2014. Langmuir 30(26), 7833-7841.

Shan, Y., Yang, Y., Cao, Y., Yin, H., Long, N.V., Huang, Z., 2015. RSC Adv. 5(44), 34737-34743.

Shen, C., Hui, C., Yang, T., Xiao, C., Tian, J., Bao, L., Chen, S., Ding, H., Gao, H., 2008. Chem. Mater. 20(22), 6939-6944.

Shi, M., Zheng, J., Tan, Y., Tan, G., Li, J., Li, Y., Li, X., Zhou, Z., Yang, R., 2015. Anal. Chem. 87(5), 2734-2740.

Smith, W., 2008. Chem. Soc. Rev. 37(5), 955-964.

Su, J., Zhang, Y., Xu, S., Wang, S., Ding, H., Pan, S., Wang, G., Li, G., Zhao, H., 2014. Nanoscale 6(10), 5181-5192.

Sun, Z., Liang, P., 2008. Microchim. Acta 162(1-2), 121-125.

Syoufian, A., Satriya, O.H., Nakashima, K., 2007. Catal. Commun. 8(5), 755-759.

Tan, E.-Z., Yin, P.-G., You, T.-t., Wang, H., Guo, L., 2012. ACS Appl. Mater. Interfaces 4(7), 3432-3437.

Themelis, D.G., Kika, F.S., Economou, A., 2006. Talanta 69(3), 615-620.

Tsoutsi, D., Guerrini, L., Hermida-Ramon, J.M., Giannini, V., Liz-Marzán, L.M., Wei, A., Alvarez-Puebla, R.A., 2013. Nanoscale 5(13), 5841-5846.

Tsoutsi, D., Montenegro, J.M., Dommershausen, F., Koert, U., Liz-Marzán, L.M., Parak, W.J., Alvarez-Puebla, R.A., 2011. ACS Nano 5(9), 7539-7546.

Tsuyumoto, I., Maruyama, Y., 2011. Anal. Chem. 83(19), 7566-7569.

Accepted manuscript

ACCEPTED MANUSCRIPT

Wang, H. J., Du, X. M., Wang, M., Wang, T. C., Ou-Yang, H., Wang, B., Zhu, M. T., Wang, Y., Jia, G., Feng, W. Y., 2010. Talanta 81(4), 1856-1860.

Wang, H., Levin, C.S., Halas, N.J., 2005. J. Am. Chem. Soc. 127(43), 14992-14993.

Wang, L., Wang, L., Xia, T., Dong, L., Chen, H., Li, L., 2004. Spectrochimi. Acta, Part A 60(11), 2465-2468.

Wang, X., Yang, T., Li, X., Jiao, K., 2011. Biosens. Bioelectron. 26(6), 2953-2959.

Wu, X., Xu, Y., Dong, Y., Jiang, X., Zhu, N., 2013. Anal. Methods 5(2), 560-565.

Xiao, J., Meng, Y., Zhang, P., Wen, W., Liu, Z., Zhang, T., 2012. Laser Phys. 22(10), 1481-1488.

Yoon, I., Kang, T., Choi, W., Kim, J., Yoo, Y., Joo, S. W., Park, Q. H., Ihee, H., Kim, B., 2008. J. Am. Chem. Soc. 131(2), 758-762.

Yu, J., Zhang, L., Cheng, B., Su, Y., 2007. J. Phys. Chem. C 111(28), 10582-10589.

Zhang, B., Wang, H., Lu, L., Ai, K., Zhang, G., Cheng, X., 2008. Adv. Funct. Mater. 18(16), 2348-2355.

Zhang, L., Chang, H., Hirata, A., Wu, H., Xue, Q. K., Chen, M., 2013. ACS nano 7(5), 4595-4600.

Zhang, L., Xu, C., Li, B., 2009. Microchim. Acta 166(1-2), 61-68.

Zhang, M., Zhao, A., Wang, D., Sun, H., 2015. Analyst 140(2), 440-448.

Zhang, X., Servos, M.R., Liu, J., 2012. J. Am. Chem. Soc. 134(24), 9910-9913.

Zheng, J., Bai, J., Zhou, Q., Li, J., Li, Y., Yang, J., Yang, R., 2015. Chem. Commun. 51(30), 6552-6555.

Zhu, J., Peng, H., Marshall, A., Barnett, D., Nix, W., Cui, Y., 2008. Nat. Nanotechnol. 3(8), 477-481.

Zou, X., Silva, R., Huang, X., Al-Sharab, J.F., Asefa, T., 2013. Chem. Commun. 49(4), 382-384.

Highlights

- A simple method for ultrasensitive detection of Cr(VI) based on glutathione functionalized TiO_2@Ag NPs SERS sensor was developed.
- The TiO_2@Ag NPs exhibits large SERS enhancement factors, and can serve as recyclable SERS-active substrates.
- The method has a good linearity in the range from 10 nM to 2 μM for Cr(VI) with a detection limit of ca. 1.45 nM.
- It features excellent selectivity to Cr(VI) over other interfering metal ions, and good application in water samples.

Accepted manuscript